Journal of Southeast University (English Edition) Vol. 32, No. 1, pp. 58 - 66 Mar. 2016 ISSN 1003—7985

Seismic performance of double-skin steel-concrete composite box piers: Part I —Bidirectional quasi-static testing

Xia Jian[1,3] Zong Zhouhong[2] Xu Chaoran[2] Li Minghong[2]

([1]School of Civil Engineering, Fuzhou University, Fuzhou 350116, China)
([2]School of Civil Engineering, Southeast University, Nanjing 210096, China)
([3]Fujian Academy of Building Research, Fuzhou 350025, China)

Abstract: To study the seismic performance of double-skin steel-concrete composite box (DSCB) piers, a total of 11 DSCB pier specimens were tested under bidirectional cyclic loading. The effects of the loading pattern, the steel plate thickness, the axial load ratio, the slenderness ratio and the aspect ratio were taken into consideration. The damage evolution process and failure modes of the tested specimens are presented in detail. Test results are also discussed in terms of the hysteretic curve, skeleton curve, ductility and energy dissipation capacity of DSCB pier specimens. It can be concluded that the hysteretic performance of DSCB piers in one direction is affected and weakened by the cyclic loading in the other direction. DSCB piers under bidirectional cyclic loading exhibit good performance in terms of load carrying capacity, ductility, and energy dissipation capacity. Overall, DSCB piers can meet the basic aseismic requirements. The research results can be taken as a reference for using DSCB piers as high piers in bridges in strong earthquake-prone areas.

Key words: double-skin steel-concrete composite box (DSCB) pier; bidirectional quasi-static testing; hysteretic curve; skeleton curve; ductility; energy dissipation capacity

DOI: 10.3969/j.issn.1003-7985.2016.01.011

Among the bridges with high piers, the cross-sections of high piers can be divided into several types, such as the concrete box section, concrete thin-wall section, steel box section, and steel-concrete composite section. Double-skin steel-concrete composite box (DSCB) piers, which are regarded as an ideal alternative for high piers of large-span bridges, have been applied to bridge substructures in strong earthquake-prone areas[1-2]. Researchers have already conducted some experimental studies on the seismic behavior of the steel-concrete composite columns or piers. Ge et al.[3-5] conducted unidirectional cyclic tests of partly concrete-filled steel box piers to study the impacts on strength, ductility and energy dissipation. Lü et al.[6] studied 12 rectangle concrete-filled steel columns in cyclic tests. Marson et al.[7] studied unidirectional cyclic tests of four circular concrete filled steel tube piers. Yang et al.[8] studied 21 concrete filled steel tubes with an elliptical hollow to ascertain the influence on confinement effect, elastic stiffness, ductility and ultimate strength. Susantha et al.[9] studied six steel piers with concrete-filled steel tubular anti-seismic components. Roeder et al.[10] conducted a pseudo-static test on 12 specimens with different connections between the concrete filled steel tubular piers and foundation. Naito et al.[11] conducted an unidirectional cyclic test on four H-shape steel-concrete composite piers and a reinforced concrete pier to make a comparison. Gajalakshmi et al.[12] studied 16 concrete filled steel tubular columns in unidirectional pseudo-static tests. Idris et al.[13-14] investigated five square and one circular concrete-filled FRP tube columns tested under constant axial compression and reversed-cyclic lateral loading. Afterwards, they also studied nine double-skin tubular columns and one concrete-filled FRP tube column under constant axial compression and reversed-cyclic lateral loading[14]. Goto et al.[15] examined the local buckling resistance behavior of thin-walled circular concrete-filled tubular columns under seismic loads by conducting bidirectional cyclic loading and bidirectional shaking table tests.

Due to the conspicuous time history and spatial distribution of earthquakes, the seismic performance of the piers in one direction will be weakened by cracking and rigidity degradation in other directions. The mutual coupling of different directions can seriously weaken the seismic capacity of the components and structures. Therefore, it is necessary to study the multi-directional performance of the structures or components under the earthquake action[16-19]. At present, in addition to the shaking table test, the multi-dimensional quasi-static test and the multi-dimensional pseudo-dynamic test are the main development directions of the structural seismic tests. For the rectangular cross-section steel-concrete composite box pier, the hysteretic behaviors in the X and Y directions are different. Therefore, there is a strong motivation to study the seismic behavior of steel-concrete composite box piers by multi-directional quasi-static tests.

In this study, 11 specimens of the DSCB pier were tested under bidirectional cyclic lateral loading, and some

Received 2015-06-01.

Biographies: Xia Jian(1970—), male, doctor, professor; Zong Zhouhong (corresponding author), male, doctor, professor, zongzh@seu.edu.cn.

Foundation items: The National Natural Science Foundation of China (No. 51178101, 51378112), the Doctoral Fund of Ministry of Education (No. 20110092110011).

Citation: Xia Jian, Zong Zhouhong, Xu Chaoran, etl al. Seismic performance of double-skin steel-concrete composite box piers: Part I —Bidirectional quasi-static testing[J]. Journal of Southeast University (English Edition), 2016, 32(1): 58 - 66. DOI: 10.3969/j.issn.1003-7985.2016.01.011.

important parameters, such as the axial load ratio, the slenderness ratio, the steel plate thickness, and the aspect ratio, were considered. The seismic behavior of the DSCB pier specimens, including the failure mode, the hysteretic curve, the skeleton curve, the ductility and the energy dissipation capacity, were analyzed and discussed.

1 Experimental Program

1.1 Design of test specimens

A laboratory test program was conducted to study the seismic performance of the proposed composite pier. The test specimens are the scaled models of the double-skin steel-concrete pier with a 6.25 m × 4.5 m rectangle section. The prototype pier was scaled down to the test specimen with a scale ratio of 1∶14 based on experimental capability. At the top of the specimen, a 540 mm × 720 mm × 700 mm concrete head block was set for the axial and lateral loading. The bottom of the test pier was fixed on a 550 mm × 800 mm × 1 300 mm concrete base block, which was bolted to the reaction floor. The filled concrete between the steel plates was C50 strength grade, and the steel plate of the standard specimen was Q235 strength grade. In total, eleven DSCB pier specimens were designed for the bidirectional quasi-static test. A schematic illustration of the test specimen is shown in Fig. 1. Tab. 1 summarizes the characteristics of the test specimens. Three specimens, U4a-A1-10-4, U4b-A1-10-4, and B4-A1-10-4, were designed as bench-mark tests. The key parameters investigated in the study include the axial load ratio, the slenderness ratio, the thickness of the steel plate, and the aspect ratio of the section. The measured concrete and steel plate properties are listed in Tab. 2 and Tab. 3.

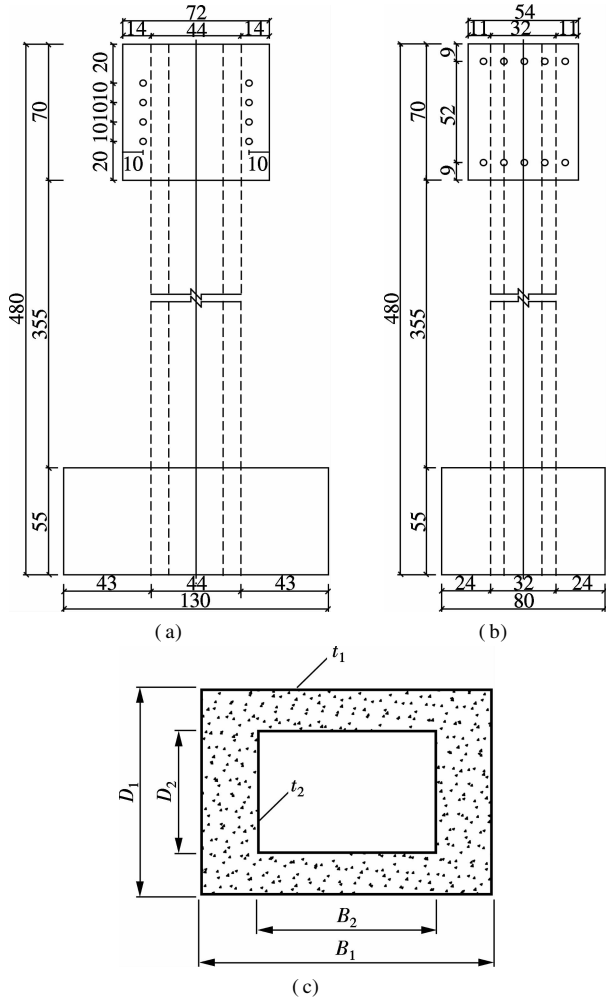

Fig. 1 Test specimens. (a) Front view of specimens (unit: cm); (b) Side view of specimens(unit: cm); (c) Section of pier specimens

Tab. 1 Dimensions and parameters of test specimens

Specimen	Height of loading/m	B_1/mm	D_1/mm	B_2/mm	D_2/mm	t_1/mm	t_2/mm	Axial load/kN	Axial load ratio
U4a-A1-10-4	4.45	440	320	260	180	4	4	460	0.10
U4b-A1-10-4	4.45	440	320	260	180	4	4	460	0.10
B4-A1-08-4	4.45	440	320	260	180	4	4	370	0.08
B4-A1-15-4	4.45	440	320	260	180	4	4	690	0.15
B3-A1-10-4	3.45	440	320	260	180	4	4	460	0.10
B5-A1-10-4	5.45	440	320	260	180	4	4	460	0.10
B4-A1-10-4	4.45	440	320	260	180	4	4	460	0.10
B4-A1-10-5	4.45	440	320	260	180	5	5	524	0.10
B4-A1-10-6	4.45	440	320	260	180	6	6	586	0.10
B4-A2-10-4	4.45	320	320	140	180	4	4	282	0.10
B4-A3-10-4	4.45	640	320	460	180	4	4	610	0.10

Note: U/B represent the unidirectional and bidirectional loading; 3/4/5 represent the height of piers; A1/A2/A3 represent three type of cross sections; 08/10/15 represent the axial load ratio.

Tab. 2 Mechanic properties of concrete samples (in average)

Concrete grade	Cubic compressive strength/MPa	Splitting tensile strength/MPa	Elastic modulus/MPa
C50	54.2	3.52	2.80×10^4

Tab. 3 Mechanic properties of steel plate samples (in average)

Thickness/mm	Yield strength/MPa	Ultimate strength/MPa	Elastic modulus/GPa	Poisson's ratio
4	303.41	392.05	201.1	0.29
5	327.27	422.45	225.0	0.28
6	286.36	386.97	209.0	0.27

1.2 Test setup

Figs. 2(a) to (c) shows the schematic illustration of the test setup. The specimen was anchored to the reaction floor by high strength bolts. To simulate actual seismic loading patterns, bidirectional lateral cyclic loads combined with a vertical compressive axial load were applied to the specimens. The horizontal lateral loads were applied using MTS hydraulic actuators, and the vertical compressive axial load was applied using a 1 000 kN hydraulic jack to maintain a uniform axial load on the specimens. A photograph of the test setup is given in Fig. 2(d).

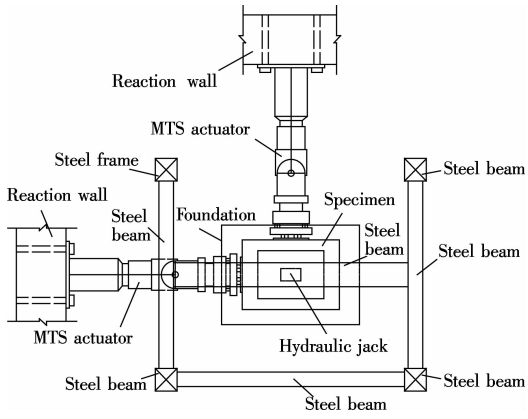

(a)

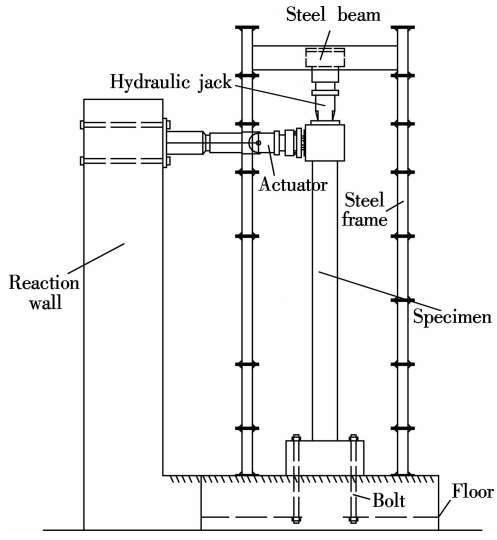

(b)

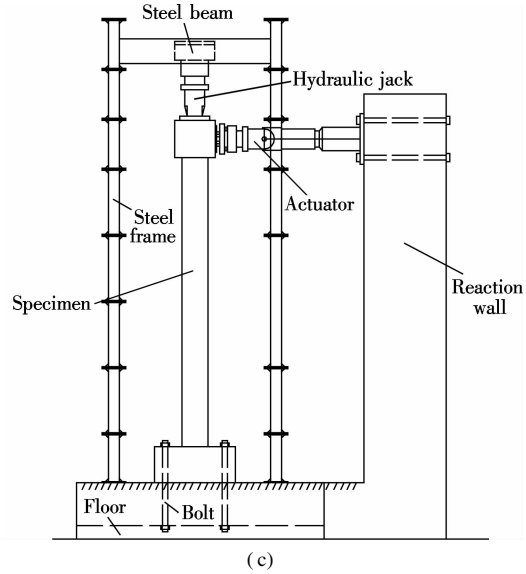

(c)

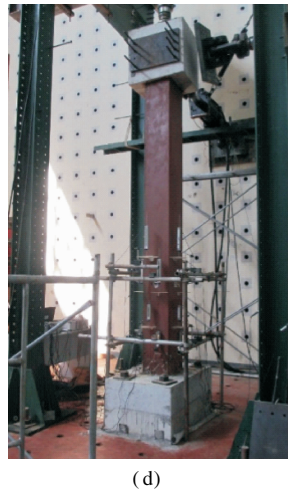

(d)

Fig. 2 Test setup. (a) Plan view; (b) Side view in *Y* direction; (c) Side view in *X* direction; (d) Photograph of the test setup

1.3 Load sequence and measurements arrangement

Specimen U4a-A1-10-4 and U4b-A1-10-4 were subjected to a unidirectional lateral cyclic loading. The other specimens were subjected to a synchronously bidirectional lateral cyclic loading as shown in Fig. 3(a). The test loading was determined using the displacement control at the loading point. The ratio of the displacement in the *X* direction to that in the *Y* direction is 1∶1. The loading sequence is shown in Fig. 3(b). The test specimen was considered to have failed when the lateral load dropped to 85% of the historical maximum value, or the test would be terminated when the maximum stroke of actuator had been reached. In order to measure the curvature of the yield zone, four displacement meters are mounted on each side of the test specimen, as shown in Fig. 4. Each side of the interior steel plate was stuck on with three strain gauges while each side of the exterior steel plate was stuck on with nine strain gauges to measure the strain of the steel plate. The locations of the strain gauges are shown in Fig. 5.

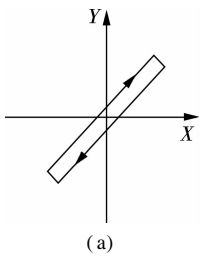

(a)

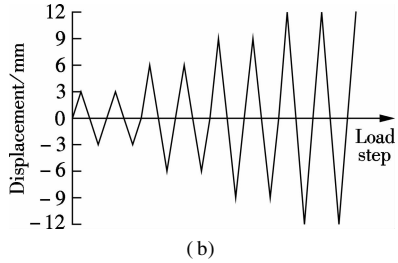

(b)

Fig. 3 Bidirectional cyclic loading pattern. (a) Synchronously bidirectional lateral cyclic loading pattern; (b) Loading sequence

Fig. 4 Location of displacement meters

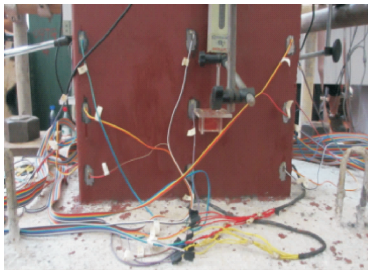

Fig. 5 Location of strain gauges

2 Experimental Results

2.1 Failure modes

For all the test specimens under the bidirectional cyclic loading, crisp sound was first heard during the cycles between the second displacement level (i.e. the maximum displacement 6 mm) and the fourth displacement level (i.e. maximum displacement 12 mm), indicating that separation between the steel plate and concrete occurred. With the increase of the displacement, slight local plate buckling deformation was observed in the region close to the foot of the pier and then progressively grew during reversed loading. As the displacement continuously rose, transverse cracking in the plate material of the common edges (see Figs. 6(c) and (d)) or vertical cracking in the welding area began to be seen (see Fig. 6(e)). These phenomena indicated that the foot of the pier started to produce a plastic hinge. Eventually, the specimen lost its lateral load resistance after the cracking became considerable and the loading was then terminated, which also demonstrated the formation of the plastic hinge. In those test specimens, local buckling only took place in plates near the base of the piers (see Figs. 6(a) and (b)). It should be noted that specimen B3-A1-10-4 and B5-A1-10-4 had a different slenderness ratio from the other specimens, and the three buckling regions formed on the sides (see Fig. 6(f)). On the other hand, for specimen U4a-A1-10-4 and U4b-A1-10-4 under a unidirectional cyclic loading, crisp sound and local plate buckling appeared only on the two sides along with the loading direction. After testing, all the specimens were cut off at the height of 500 mm. The bond condition between the concrete and the steel plate was still good above the cut. At the height of the buckling regions in the exterior steel plates, each side of the interior plates had also buckled (see Fig. 6(g)), and near the common edges of the compressed sides, the concrete was heavily crushed (see Fig. 6(h)).

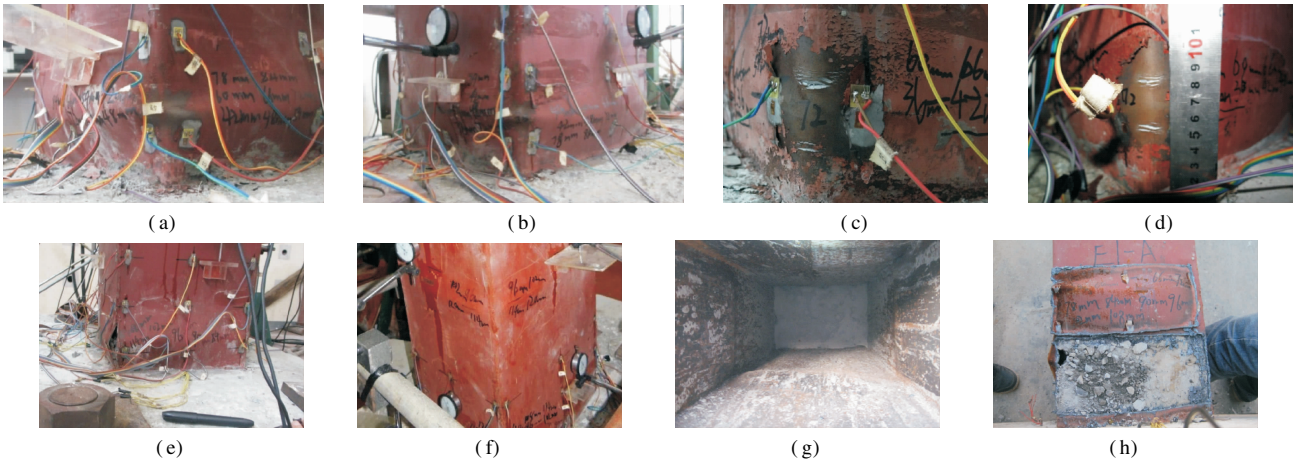

Fig. 6 Typical failure appearances. (a) Local buckling on side *A* and side *D* (specimen B4-A1-15-4); (b) Local buckling on side *B* and side *C* (specimen B4-A1-15-4); (c) Cracks at common edge of side *A* and side *D* (specimen B5-A1-10-4); (d) Cracks at common edge of side *B* and side *C* (specimen B5-A1-10-4); (e) Weld crack of U4b-A1-10-4; (f) Three buckling regions of B3-A1-10-4; (g) Local buckling of inner steel plates; (h) Crushed concrete after the test

2.2 Hysteretic curves and skeleton curves

Fig. 7 shows a part of the horizontal load versus displacement hysteretic curves of the specimens obtained from the tests. As seen in the figures, the absolute value of the maximum and minimum load in the *X* direction is larger than that in the *Y* direction at each loading level. The hysteretic loops of the piers transform from line to spindle, to bow and finally to S-shape under lateral cyclic loading. Furthermore, the hysteretic loops in the *X* direction were pinched more obviously than the loops in the *Y* direction.

The envelope curves of the horizontal load-displacement hysteretic curves are shown in Fig. 8. It sketches the increasing path of the peak load value for each displacement level, which can clearly indicate the variations in the strength, stiffness, and ductility of pier specimens. In general, it can be seen that the envelope curves in the *X* direction clearly have larger loading strength than that in the *Y* direction. Additionally, the following significant facts can be observed from Fig. 8.

Comparisons among specimen U4a-A1-10-4, U4b-A1-10-4, and B4-A1-10-4 indicate that the lateral strength and ductility capacity are clearly affected by a horizontal load applied in another direction. As shown in Figs. 8(a) and (b), the absolute values of both the maximum load and displacement under unidirectional loading are larger than those under bidirectional loading. Comparing specimen B4-A1-10-4 with specimen U4a-A1-10-4 and U4b-A1-10-4, the lateral strength decreases by approximately 25% and 46% in the *X* direction and *Y* direction, respec-

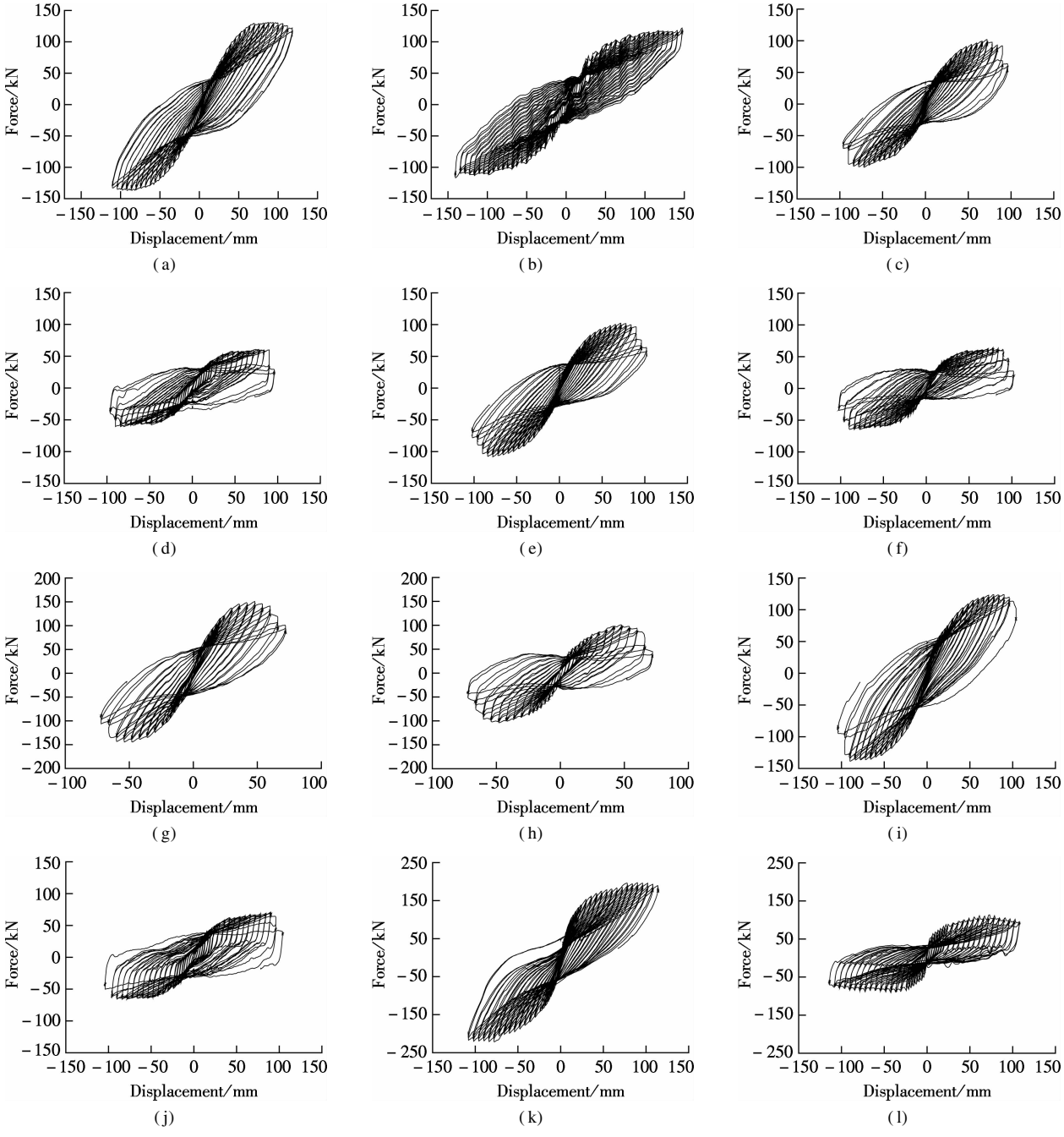

Fig. 7 Horizontal load-displacement hysteretic curves of test specimens. (a) U4a-A1-10-4; (b) U4b-A1-10-4; (c) B4-A1-10-4 in *X* direction; (d) B4-A1-10-4 in *Y* direction; (e) B4-A1-15-4 in *X* direction; (f) B4-A1-15-4 in *Y* direction; (g) B3-A1-10-4 in *X* direction; (h) B3-A1-10-4 in *Y* direction; (i) B4-A1-10-5 in *X* direction; (j) B4-A1-10-5 in *Y* direction; (k) B4-A3-10-4 in *X* direction; (l) B4-A3-10-4 in *Y* direction

tively. The ultimate displacement of specimen B4-A1-10-4 in the *X* direction decreases by 15.8% compared with the specimen U4a-A1-10-4, and the ultimate displacement of specimen B4-A1-10-4 in the *Y* direction decreases by 37.5% compared with the specimen U4b-A1-10-4. This means that the seismic performance of DSCB pier specimens under unidirectional cyclic loading cannot fully reflect that under bidirectional cyclic loading.

Comparing specimen B4-A1-15-4, B4-A1-08-4, and B4-A1-10-4 (see Figs. 8(c) and (d))), the seismic behavior in the *Y* direction is almost the same before reaching the peak load despite of the different axial load ratios. Nonetheless, with the axial load ratio increasing, the ultimate displacement has a slight decrease. For the seismic behavior in the *X* direction, the ultimate displacement of specimen B4-A1-08-4 is approximately 13% smaller than that of specimen B4-A1-10-4, while the maximum load of the former increases by approximately 15% compared with the latter. This phenomenon is due to the fact that when the P-Δ effect becomes obvious, concrete is crushed seriously and the slip between concrete and steel grows in the specimens with a larger axial load ratio.

By comparison among specimens B3-A1-10-4, B5-A1-10-4, and B4-A1-10-4, it can be seen from Figs. 8(e) and (f) that the slender pier specimen has smaller ultimate loading capacity but a much larger and more stable

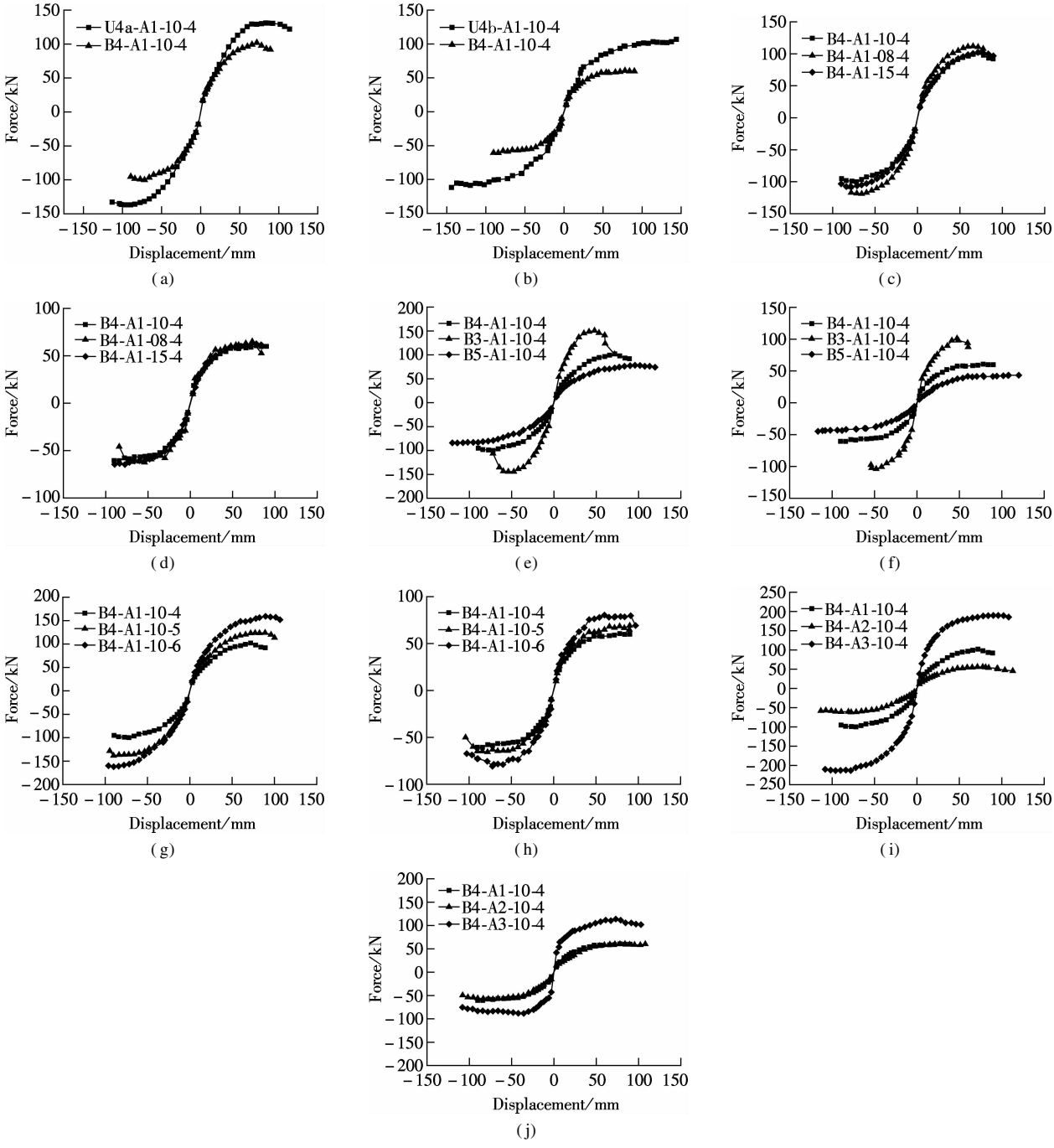

Fig. 8 Influences of different design parameters on skeleton curves. (a) Loading patterns in *X* direction; (b) Loading patterns in *Y* direction; (c) Axial load ratio in *X* direction; (d) Axial load ratio in *Y* direction; (e) Slenderness ratio in *X* direction; (f) Slenderness ratio in *Y* direction; (g) Thickness of the steel plate in *X* direction; (h) Thickness of the steel plate in *Y* direction; (i) Aspect ratio in *X* direction; (j) Aspect ratio in *Y* direction

post-peak deformation. For example, the ultimate loading capacity of specimen B3-A1-10-4 is almost 2 times that of specimen B5-A1-10-4, but the ultimate displacement of the former is merely 50% that of the latter.

As shown in Figs. 8(g) and (h), comparisons of specimen B4-A1-10-5 and B4-A1-10-6 with specimen B4-A1-10-4 indicate that the maximum loads were increased by approximately 30% and 60% in the *X* direction when the steel ratios were increased from 10.2% to 12.8% and 15.3%, respectively, while in the *Y* direction the increases were approximately 13% and 34%. This is because only slight local buckling occurred in the base panels with thicker steel in the failure stage. On the other hand, there were slight increases in the ultimate displacement along with the increase of steel ratio. Compared with specimen B4-A1-10-4, the increases of ultimate displacement of specimen B4-A1-10-5 and B4-A1-10-6 were only approximately 4.2% and 12.5% in the *X* direction, while in the *Y* direction they were approximately 11% and 13.3%, respectively.

Figs. 8(i) and (j) show that a smaller size of the section in the *X* direction has a negative effect on the maximum loading capacity while offering larger ultimate displacement. For example, compared with specimen B4-

A1-10-4 (aspect ratio 1.375) in the *X* direction, the maximum loading capacity of specimen B4-A2-10-4 (aspect ratio 1) decreased by approximately 40%, while its ultimate displacement was increased by approximately 13%. This can be attributed to the smaller inertia moment and stiffness of the pier with a smaller section.

2.3 Ductility behavior

Ductility is an important consideration in aseismic design. There are several ways to assess the ductility capacity of a structure. One method is to define the ductility factor as

$$\mu = \frac{\Delta_u}{\Delta_y} \tag{1}$$

where Δ_u is the ultimate displacement, which is defined as the displacement that occurs when the lateral load-carrying capacity degrades to 85% of the maximum load P_m, or the maximum displacement in the envelope curve when the previous condition cannot be satisfied; Δ_y is the yield displacement corresponding to the yield point of the test specimen. The bi-linear energy equivalent method is employed to determine the yield point *Y* as presented in Fig. 9, in which the intersection point *B* of line *OA* and *DC* can make the sum of area S_1 and S_3 be equal to area S_2, and assure that S_2 is the smallest.

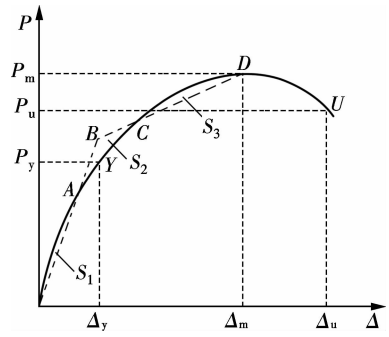

Fig. 9 Definition of yield point

Tab. 4 and Tab. 5 summarize the ductility factor μ of all specimens using the envelope curves of horizontal load-displacement hysteretic loops in Fig. 7. The minimum ductility factors of the test specimens are all larger than 2.9, which indicates that the DSCB piers have good ductility capacity.

Compared with U4a-A1-10-4 and U4b-A1-10-4 under unidirectional loading, the ductility factor of B4-A1-10-4 shows a little decrease in the *X* direction and *Y* direction, respectively. The width to thickness ratio of the steel plate has little effect on the ductility factor of the specimen in the *X* direction, while the ductility factors in the *Y* direction increase significantly with the decrease in the width to thickness ratio of the steel plate. The ductility factor of the specimen in the *X* direction is increased slightly with the height increasing from 3.45 to 5.45 m, but in the *Y* direction, the ductility factor has a noticeable decrease from 5.0 to 2.9. When the axial load ratio becomes larger, the ductility factor of the specimen is reduced in the *X* direction, but it is increased in the *Y* direction. With the increase in the aspect ratio, the ductility factor of the specimen increases in both directions. As the foundation of specimen B4-A3-10-4 cracked, the test results

Tab. 4 Characteristic point of skeleton curve and ductility factor (in *X* direction)

Specimen	Yield point *Y*		Peak point *D*		Ultimate point *U*		μ
	Δ_y/mm	P_y/kN	Δ_m/mm	P_m/kN	Δ_u/mm	P_u/kN	
U4a-A1-10-4	27.80	115.75	84.02	129.37	114.03	121.72	4.101
B4-A1-10-4	23.45	75.17	72.02	96.65	89.00	91.00	3.795
B4-A1-10-5	26.32	113.97	87.03	126.66	100.02	98.49	3.800
B4-A1-10-6	28.40	123.09	90.03	155.18	108.02	128.10	3.804
B3-A1-10-4	19.30	119.66	54.00	141.00	60.00	141.00	3.109
B5-A1-10-4	30.30	63.67	102.00	78.00	120.00	74.00	3.960
B4-A1-08-4	20.15	87.77	66.02	111.41	77.00	107.00	3.821
B4-A1-15-4	26.05	67.79	72.04	101.47	89.00	96.00	3.417
B4-A2-10-4	30.35	48.59	72.02	57.76	108.04	49.99	3.560
B4-A3-10-4	21.50	165.68	90.02	201.57	108.03	200.05	5.025

Tab. 5 Characteristic point of skeleton curve and ductility factor (in *Y* direction)

Specimen	Yield point *Y*		Peak point *D*		Ultimate point *U*		μ
	Δ_y/mm	P_y/kN	Δ_m/mm	P_m/kN	Δ_u/mm	P_u/kN	
U4b-A1-10-4	36.10	86.51	144.03	103.94	144.03	103.94	3.990
B4-A1-10-4	23.95	51.36	84.03	56.14	90.02	60.00	3.759
B4-A1-10-5	19.00	53.02	69.03	63.76	89.00	65.00	4.684
B4-A1-10-6	14.25	54.16	60.03	75.13	96.00	69.00	6.737
B3-A1-10-4	12.00	68.25	48.00	101.00	60.00	87.00	5.000
B5-A1-10-4	41.30	39.74	120.00	43.00	120.00	43.00	2.906
B4-A1-08-4	23.50	56.12	54.02	58.43	84.02	52.00	3.575
B4-A1-15-4	22.00	50.92	84.00	61.00	84.00	61.00	3.818
B4-A2-10-4	29.20	51.03	72.03	56.52	108.03	54.60	3.700
B4-A3-10-4	6.25	68.95	60.04	87.77	108.03	79.00	17.285

of specimen B4-A3-10-4 were only taken as a reference.

2.4 Energy dissipation capacity

Energy dissipation capacity is also one of the most important considerations in aseismic design. The cumulative dissipated energy of the test specimen can be calculated by adding up the enclosed area in each hysteretic loop. Fig. 10 illustrates the relationship between the dissipated energy and lateral displacement. Each point in the graph is the cumulative dissipated energy up to the second loading cycle of the current displacement level.

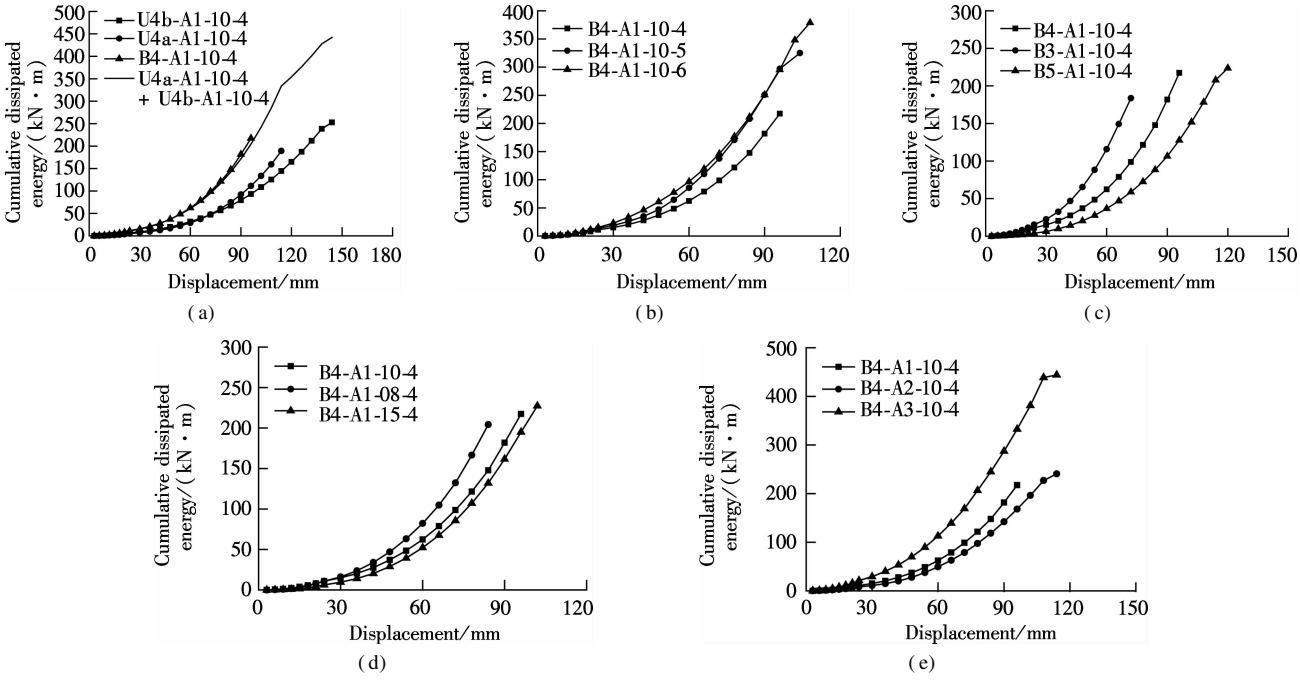

Fig. 10 Influence of different design parameters on the cumulative dissipated energy. (a) Different loading patterns; (b) Width to thickness ratio of the steel plate; (c) Slenderness ratio; (d) Axial load ratio; (e) Aspect ratio

Fig. 10(a) shows that specimen B4-A1-10-4 under bidirectional loading can dissipate more energy than U4a-A1-10-4 and U4b-A1-10-4 under unidirectional loading at the same displacement level. Furthermore, the cumulative dissipated energy of B4-A1-10-4 is a little larger than the sum of the dissipated energy of U4a-A1-10-4 and U4b-A1-10-4.

It is apparent from Figs. 10(b) to (d) that the cumulative dissipated energy decreases with the increase of the width to thickness ratio of the steel plate, the slenderness ratio, and the axial load ratio, while Fig. 10(e) demonstrates that the energy dissipation capacity is improved as the aspect ratio of the section increases.

3 Conclusions

1) The hysteretic behavior of the DSCB pier specimen in one direction is significantly affected by the lateral load applied in another direction. The hysteretic behavior under unidirectional loading cannot fully reveal the seismic performance of DSCB piers under the multi-directional loading pattern.

2) The influences of the slenderness ratio, the thickness of steel plate, and the aspect ratio on the skeleton curve are more obvious than the axial load ratio (Axial load ratio is less than 0.15). The slender pier specimen has a smaller ultimate loading capacity, but much better ductility capacity. The increase in the thickness of steel plate can enhance the strength of the specimen, while the ultimate displacement varies little. The ultimate loading capacity of the specimen increases with the increase in the aspect ratio, while the ultimate displacement decreases.

3) The DSCB pier specimen under bidirectional loading can dissipate more energy than those under unidirectional loading at the same displacement level. The cumulative dissipated energy decreases with the increase in the width to thickness ratio of the steel plate, the slenderness ratio, and the axial load ratio, while it increases as the aspect ratio of the section increases.

4) DSCB piers under bidirectional cyclic loading have good performance in terms of load carrying capacity, ductility, and energy dissipation capacity, and they can meet the basic aseismic requirements.

References

[1] Zong Z H, Xia J, Xu C R. Seismic study of high piers of large-span bridge: An overview and research developments[J]. *Journal of Southeast University* (*Natural Science Edition*), 2013, **43**(2): 445 − 452. (in Chinese)

[2] Hu Y. Experimental research and nonlinear analysis on concrete filled steel tubular laminated laced columns and nonperformance of high pier [D]. Chengdu: Civil Engineering College, Southwest Jiaotong University, 2010. (in Chinese)

[3] Usami T, Ge H B. Ductility of concrete-filled steel box columns under cyclic loading [J]. *Journal of Structural*

Engineering, 1994, **120**(7): 2021 - 2040.
[4] Ge H B, Usami T. Cyclic tests of concrete-filled steel box columns[J]. *Journal of Structural Engineering*, 1996, **122**(10): 1169 - 1177.
[5] Usami T, Ge H B, Saizuka K. Behaviour of partially concrete-filled steel bridge piers under cyclic and dynamic loading[J]. *Journal of Constructional Steel Research*, 1997, **41**(2): 121 - 136.
[6] Lü X L, Lu W D. Seismic behavior of concrete-filled rectangular steel tubular columns under cyclic loading[J]. *Journal of Building Structures*, 2000, **21**(2): 2 - 11, 27. (in Chinese)
[7] Marson J, Bruneau M. Cyclic testing of concrete-filled circular steel bridge piers having encased fixed-based detail[J]. *Journal of Bridge Engineering*, 2004, **9**(1): 14 - 23.
[8] Yang H, Lam D, Gardner L. Testing and analysis of concrete-filled elliptical hollow sections [J]. *Engineering Structures*, 2008, **30**(12): 3771 - 3781. DOI: 10.1016/j.engstruct.2008.07.004.
[9] Susantha K A S, Aoki T, Hattori M. Seismic performance improvement of circular steel columns using precompressed concrete-filled steel tube [J]. *Journal of Constructional Steel Research*, 2008, **64**(1): 30 - 36. DOI: 10.1016/j.jcsr.2007.05.001.
[10] Roeder C W, Lehman D E. Research on rapidly constructed CFT bridge piers suitable for seismic design [C]// *TCLEE* 2009: *Lifeline Earthquake Engineering in a Multi-Hazard Environment*. Oakland, USA, 2009: 681 - 694.
[11] Naito H, Akiyama M, Suzuki M. Ductility evaluation of concrete-encased steel bridge piers subjected to lateral cyclic loading [J]. *Journal of Bridge Engineering, ASCE*, 2011, **16**(1): 72 - 81.
[12] Gajalakshmi P, Helena H J. Behaviour of concrete-filled steel columns subjected to lateral cyclic loading[J]. *Journal of Constructional Steel Research*, 2012, **75**(1): 55 - 63. DOI: 10.1016/j.jcsr.2012.03.006.
[13] Idris Y, Ozbakkaloglu T. Seismic behavior of high-strength concrete-filled FRP tube columns[J]. *Journal of Composite Construction*, 2013, **17**(6): 04013103.
[14] Ozbakkaloglu T, Idris Y. Seismic behavior of FRP-high-strength concrete—steel double-skin tubular columns[J]. *Journal of Structural Engineering*, 2014, **140**(6): 04014019.
[15] Goto Y, Ebisawa T, Lü X L. Local buckling restraining behavior of thin-walled circular CFT columns under seismic loads[J]. *Journal of Structural Engineering*, 2014, **140**(5): 04013105.
[16] Takizawa H, Aoyama H. Biaxial effects in modelling earthquake response of RC structures[J]. *Earthquake Engineering & Structural Dynamics*, 1976, **4**(6): 523 - 552.
[17] Bousias S N, Verzeletti G, Fardis M N, et al. Load-path effects in column biaxial bending with axial force[J]. *Journal of Engineering Mechanics*, 1995, **121**(5): 596 - 605.
[18] Chang S Y. Experimental studies of reinforced concrete bridge columns under axial load plus biaxial bending[J]. *Journal of Structural Engineering*, 2010, **136**(1): 12 - 25.
[19] Rodrigues H, Varum H, Arêde A, et al. A comparative analysis of energy dissipation and equivalent viscous damping of RC columns subjected to uniaxial and biaxial loading[J]. *Engineering Structures*, 2012, **35**(1): 149 - 164. DOI: 10.1016/j.engstruct.2011.11.014.

双壁钢箱混凝土组合墩柱抗震性能研究Ⅰ:双向拟静力试验

夏 坚[1,3] 宗周红[2] 徐焯然[2] 李明鸿[2]

([1] 福州大学土木工程学院,福州 350116)
([2] 东南大学土木工程学院,南京 210096)
([3] 福建省建筑科学研究院,福州 350025)

摘要:为研究双壁钢箱混凝土组合墩柱(DSCB 墩柱)的抗震性能,对 11 个 DSCB 墩柱试件进行了双向拟静力试验,考虑了加载模式、钢板厚度、轴压比、长细比、截面长宽比等主要因素对 DSCB 墩柱抗震性能的影响.给出了试件的主要损伤演化过程和破坏模式,并从滞回曲线、骨架曲线、延性和耗能能力等方面对试验结果进行了分析.结果表明:水平双向加载下,DSCB 墩柱一个方向的损伤劣化会加剧另一个方向的损伤;DSCB 墩柱在水平双向荷载作用下,具有良好的强度、延性和耗能能力,能够满足强震区高墩桥梁的抗震要求.该研究可为 DSCB 墩柱在强震地区高墩桥梁中的应用提供依据.

关键词:双壁钢箱混凝土组合墩柱;双向拟静力试验;滞回曲线;骨架曲线;延性;耗能能力
中图分类号:U443.22